

## Structural and Conductivity Studies of YDC-CYC Electrolyte

S. RAMESH<sup>1\*</sup> and C. VISHNUVARDHAN REDDY<sup>2</sup>

<sup>1</sup>School of Physics, University of Hyderabad, Hyderabad-500 046, India

<sup>2</sup>Department of Physics, Osmania University, Hyderabad-500 007, India

\*Corresponding author: Fax: +91 40 230110227; E-mail: ramesh.ou1@gmail.com

(Received: 10 September 2011;

Accepted: 6 June 2012)

AJC-11548

The effect of Ca addition (0-9 wt %) on the structure, densification, conductivity and thermal expansion of  $Ce_{0.8}Y_{0.2}O_2$  was studied. The  $Ce_{0.8}(Y_{1-x}Ca_x)_{0.2}O_2$  ( $x = 0, 0.15, 0.3$  and  $0.45$ ) samples were prepared through the sol-gel process. Structure and phase was confirmed by XRD. Dense  $Ce_{0.8}(Y_{1-x}Ca_x)_{0.2}O_2$  ceramics were obtained through sintering the pellets at  $1300\text{ }^\circ\text{C}$ . The surface morphology of the sintered pellets was analyzed using SEM. Thermal expansion was studied by dilatometer. The two-probe A.C. impedance spectroscopy was used to study the grain ionic conductivity of doped and co-doped ceria in the temperature range  $300\text{-}700\text{ }^\circ\text{C}$ . The composition  $Ce_{0.8}Y_{0.17}Ca_{0.03}O_2$  showed improved grain ionic conductivity and minimum activation energy.

**Key Words:** Ceramics, Sol-gel process, Impedance spectroscopy, Ionic conductivity.

### INTRODUCTION

Solid oxide fuel cells (SOFCs) are the energy converters *i.e.*, they convert chemical energy into electrical energy. They have known for high efficient and clean energy conversion devices. Yttria-stabilized zirconia (YSZ) is a standard electrolyte for solid oxide fuel cell applications. High operating temperature ( $> 1,000\text{ }^\circ\text{C}$ ) is required to increase the ionic conductivity of yttria-stabilized zirconia. However, such high operating temperatures yields problems like thermal mismatch between cell components, chemical instability, selection of materials *etc.*<sup>1-4</sup>. Therefore, there remains a strong motivation to search for new improved oxide-ion electrolytes in the intermediate temperature ( $400\text{-}700\text{ }^\circ\text{C}$ )<sup>1</sup>.

The literature survey<sup>5-12</sup> shows that the co-doping could improve the ionic conductivity. Solid oxide fuel cell applications require fully dense electrolyte material. To achieve such high densification in ceria based oxide prepared by solid-state route, normally high sintering temperature required ( $> 1500\text{ }^\circ\text{C}$ )<sup>13</sup>. However, sintering temperature can be reduced by selection of suitable method for material preparation<sup>14</sup>.

In the present study  $Y^{3+}$  and  $Ca^{2+}$  co-doped ceria based materials  $Ce_{0.8}Y_{0.2}O_2$  (YDC),  $Ce_{0.8}(Y_{0.85}Ca_{0.15})_{0.2}O_2$  (CYC15),  $Ce_{0.8}(Y_{0.7}Ca_{0.3})_{0.2}O_2$  (CYC30) and  $Ce_{0.8}(Y_{0.55}Ca_{0.45})_{0.2}O_2$  (CYC45) are prepared and characterized. The main aim of the present study is to investigate the effect of Ca on the crystal structure, sintering temperature on densification, electrical properties, activation energy and thermal expansion of co-doped ceria materials.

### EXPERIMENTAL

The polycrystalline samples with the general formula  $Ce_{0.8}(Y_{1-x}Ca_x)_{0.2}O_2$  ( $0, 0.15, 0.03$  and  $0.45$ ) were synthesized through the sol-gel process as to make different metal ions mixed more homogeneously. High purity cerium nitrate hexahydrate [ $Ce(NO_3)_3 \cdot 6H_2O$ ] ( $\geq 99.9$  wt % Sigma-Aldrich), yttrium nitrate hexahydrate ( $Y(NO_3)_3 \cdot 6H_2O$ ) ( $\geq 99.9$  wt % Sigma-Aldrich) and calcium nitrate tetrahydrate [ $Ca(NO_3)_2 \cdot 4H_2O$ ] ( $\geq 99.9$  wt % Sigma-Aldrich) were used as starting materials. Stoichiometric amounts of nitrates were dissolved in de-ionized water under continuous stirring in a beaker. Citric acid was added to the solution in 1:1 molar ratio and then adding the ammonium hydroxide drop by drop to the solution the pH was adjusted to  $\approx 7$ . The transparent solution was stirred at  $65\text{ }^\circ\text{C}$  until a thick homogeneous solution was formed. Ethylene glycol was added to the solution in the molar ratio 1:1.2 and heated at  $80\text{ }^\circ\text{C}$  until a brownish sponge type viscous gel was yielded. After, the gel was placed in a burner; auto ignition was completed with in a few seconds, giving rise to a light yellow colored ash, which was calcined at  $600\text{ }^\circ\text{C}$  for 2 h to remove the carbonaceous materials and to obtain the most stable mixed oxide phase. The oxidation of  $Ce^{3+}$  to  $Ce^{4+}$  occurred during this stage<sup>15</sup>. The resultant ash was ground in agate mortar to get a fine homogeneous powder.

Further the powders were pressed uni-axially with the help of hydraulic press under a continuous pressure of 20 Mpa for 5 min into a circular pellet using a stainless steel die of

dimensions 10 mm × 2 mm and then the green pellets were sintered in air at 1300 °C for 5 h with a programmed heating rate of 5 °C/min. Densities of the sintered samples were measured in water using the Archimedes method and calculated densities of sintered samples were more than 96 % of the theoretical density.

X-Ray diffraction patterns of the test samples were obtained by PANalytical X'Pert Pro X-ray diffractometer (XRD) using  $\text{CuK}_\alpha$  radiation. Lattice parameter was calculated using XLAT software. The surface morphology of the samples was observed using the scanning electron microscope ZEISS (FE-SEM).

Electrical impedance ( $Z$ ) and phase angle ( $\theta$ ) were measured using Agilent 4294A impedance analyzer in the measuring frequency range from 40 Hz to 1 MHz. The electrical conductivity measurements were taken at various temperatures in the range 300–700 °C in air. Silver paste was brushed to each side of the samples, which was subsequently dried (600 °C for 20 min), producing solid silver electrode on both sides of the pellet. The thermal expansion measurements were carried out with Netzsch push-rod dilatometer (DIL; Model Netzsch DIL 402 PC, Germany) using a constant heating rate of 5 °C/min in the temperature range 30–800 °C.

## RESULTS AND DISCUSSION

Fig. 1 shows XRD patterns of  $\text{Ce}_{0.8}(\text{Y}_{1-x}\text{Ca}_x)_{0.2}\text{O}_2$  powders. It can be seen that powders contain only a cubic structure with the space group (JCPDS powder diffraction File No. 34-0394). The introduction of  $\text{Y}^{3+}$  and  $\text{Ca}^{2+}$  into  $\text{Ce}^{4+}$  can cause a small shift in the ceria peaks as shown in Fig. 2. This shift is an indicative of a change in the lattice parameter. This is due to the difference in ionic radii of  $\text{Ce}^{4+}$  (0.96 Å),  $\text{Y}^{3+}$  (1.08 Å) and  $\text{Ca}^{2+}$  (1.12 Å)<sup>16</sup> in an oxide solid solution.

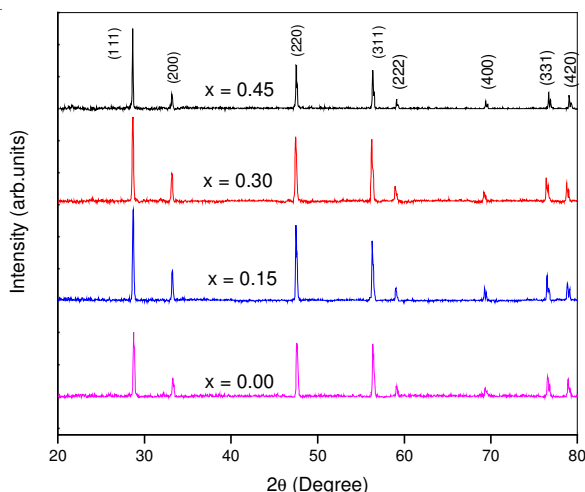


Fig. 1. XRD patterns of sintered pellets of  $\text{Ce}_{0.8}(\text{Y}_{1-x}\text{Ca}_x)_{0.2}\text{O}_2$  system

Fig. 3 shows the lattice parameter of  $\text{Ce}_{0.8}(\text{Y}_{1-x}\text{Ca}_x)_{0.2}\text{O}_2$  as a function of calcium concentration ( $x$ ). It is noticed that the lattice parameter increases linearly with an increase in the Ca amount in  $\text{Ce}_{0.8}(\text{Y}_{1-x}\text{Ca}_x)_{0.2}\text{O}_2$ . Using least-squares fitting method, a linear relationship was obtained between lattice parameter ( $a$ ) and dopant concentration ( $x$ ) and linear relation expressed as:

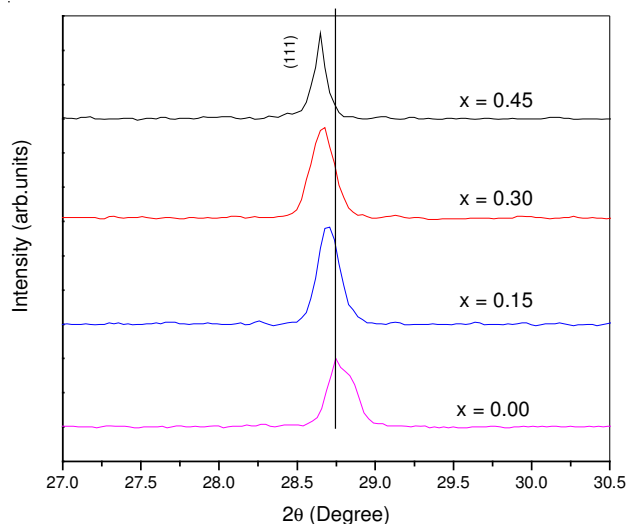


Fig. 2. Shift in (111) XRD peak position of  $\text{Ce}_{0.8}(\text{Y}_{1-x}\text{Ca}_x)_{0.2}\text{O}_2$  with increase in dopant concentration ( $x$ )

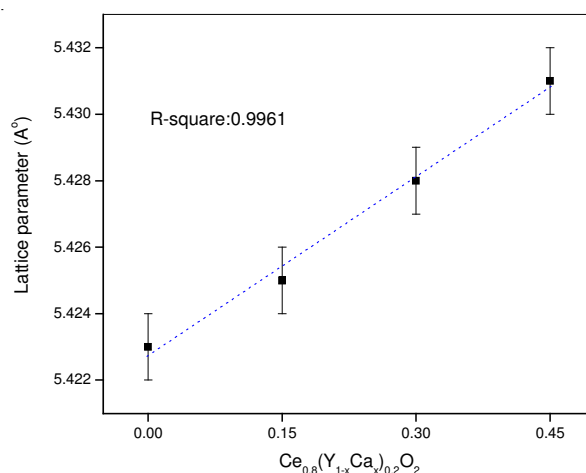


Fig. 3. Lattice parameter of  $\text{Ce}_{0.8}(\text{Y}_{1-x}\text{Ca}_x)_{0.2}\text{O}_2$  system

$$a(x) = 5.422 + 0.18x \text{ \AA} \text{ and } R^2 \text{ value is } 0.9961 \quad (1)$$

Fig. 4 shows the relative density *versus* different sintering temperatures of  $\text{Ce}_{0.8}(\text{Y}_{1-x}\text{Ca}_x)_{0.2}\text{O}_2$  specimens. It can be seen from the figure that the yttrium and calcium co-doped ceria powders shrinks very fast since its relative density increases from 63–69 % to over 96 % in the temperature range 1100–1300 °C. Fig. 5 shows the SEM picture of CYC15 sample. It is very clear that the surface of the sample is high dense. This is in good agreement with the relative density of the test samples.

A.C. impedance spectroscopy is an important tool to study the grain, grain boundary and electrode contribution to the overall ionic conductivity. The grain ionic conductivity is the fundamental material property, whereas, the total conductivity is related with the contributions of microstructure, impurity and other factors to the samples resistance<sup>17</sup>. In the present work grain ionic conductivity of different materials is reported.

Fig. 6 shows the Nyquist plots of CYC15 ceramic sample at 500 °C. It is noticed that complete semi-circle and a part of arc are clearly seen. In this case equivalent circuit  $R_b-(R-CPE)_{gb}-(R-CPE)_{el}$  was used to fit the impedance data to calculate grain ( $R_b$ ) resistance. The grain arc was not well resolved

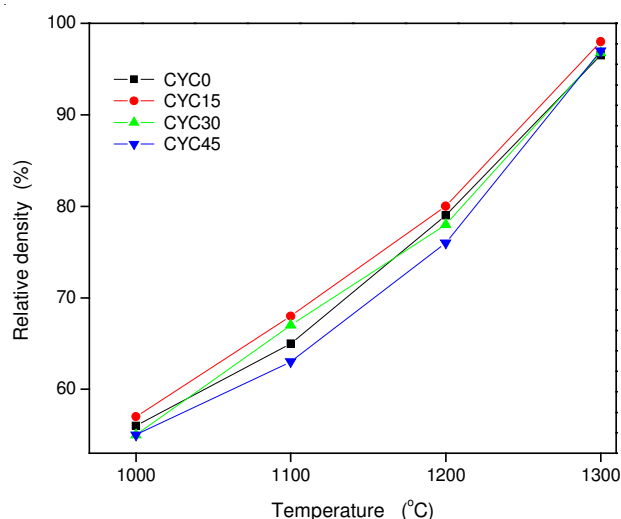


Fig. 4. Variation of relative density as a function of temperature for  $\text{Ce}_{0.8}(\text{Y}_{1-x}\text{Ca}_x)_{0.2}\text{O}_2$  system

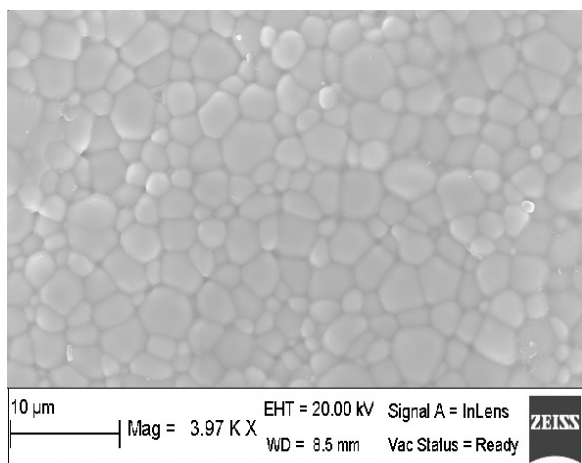


Fig. 5. SEM picture of CYC15 pellet

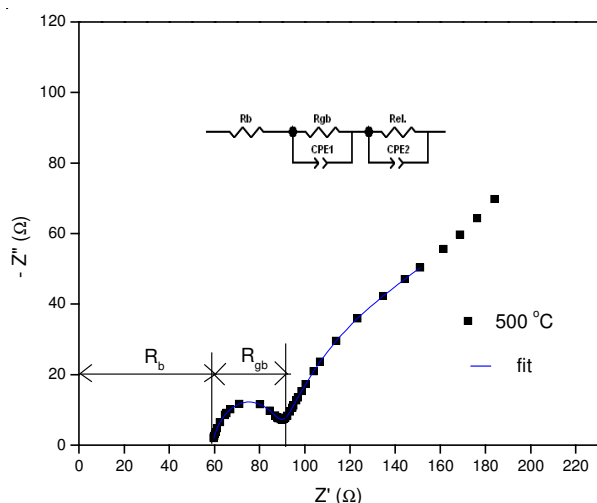


Fig. 6. Nyquist plot of CYC15 sample at 500 °C

due to decrease in relaxation time and grain arc shifts towards the higher frequency region exceeding the equipment limit (higher frequencies are required to observe grain contribution). The use of simple capacitor is not sufficient to model the electrical response of the materials due to depression of arcs

in some cases. For this purpose a constant phase element (CPE) was used to fit the results<sup>18</sup>. The main contribution of the conductivity of ceria-based compounds in air is the ionic conductivity and contribution of the electronic conductivity is negligible<sup>2,17,18</sup>. In the present investigation the measured conductivity is treated as oxide ion conductivity.

The grain ionic conductivity ( $\sigma_g$ ) is then calculated from the grain resistance ( $R_b$ ) taking into account thickness and cross sectional area  $A$  using following equation

$$\sigma = \frac{1}{RA} \quad (2)$$

The activation energy is calculated using equation,

$$\sigma = \frac{\sigma_0}{T} \exp\left(-\frac{E_0}{kT}\right) \quad (3)$$

where  $E_a$  = activation energy,  $k$  = Boltzmann constant,  $\sigma_0$  = Pre exponential factor.

Fig. 7 shows the Arrhenius plots of the grain ionic conductivity for  $\text{Ce}_{0.8}(\text{Y}_{1-x}\text{Ca}_x)_{0.2}\text{O}_2$  ceramics. Oxide vacancies ( $\text{V}_\text{O}^{\bullet\bullet}$ ) may be created in  $\text{CeO}_2$  by doping  $\text{Y}_2\text{O}_3$  or  $\text{CaO}$ <sup>1,2</sup>. These equations are written in Kroger-Vink notation<sup>2</sup>.

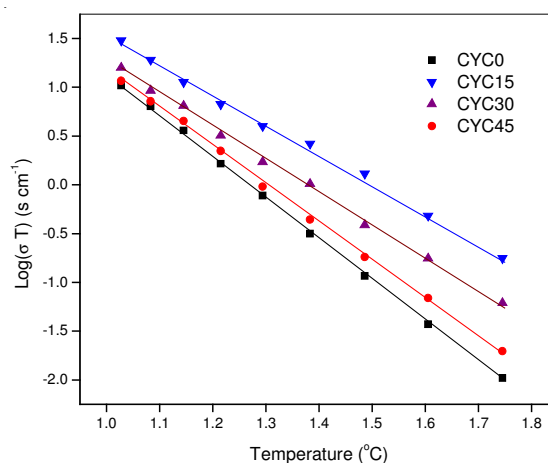
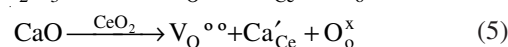
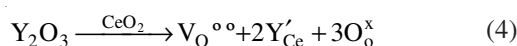


Fig. 7. Temperature dependence of grain ionic conductivity for  $\text{Ce}_{0.8}(\text{Y}_{1-x}\text{Ca}_x)_{0.2}\text{O}_2$  system



It can be seen from Fig. 7 that yttrium and calcium co-doped ceria samples showed higher conductivities for the composition CYC15, CYC30 than single doped ceria.

Fig. 8 shows the grain ionic conductivity of co-doped ceria samples at different temperatures. It can be seen that the grain ionic conductivity maximum at CYC15. After it decreases due to the formation of local defect structures, which lowers the mobile oxygen vacancy<sup>1,5</sup>. In fact, activation energy shows the reverse path (Fig. 9). The composition  $\text{Ce}_{0.8}\text{Y}_{0.17}\text{Ca}_{0.03}\text{O}_2$  (CYC15) showed highest grain ionic conductivity  $0.0309 \text{ S cm}^{-1}$  which is 2.91 orders than (YDC)  $\text{Ce}_{0.8}\text{Y}_{0.2}\text{O}_2$  ( $0.0106 \text{ S cm}^{-1}$ ) at 700 °C. These conductivity values are well compared with the reported values<sup>8,12,17</sup>. However, the ionic conductivity of the  $\text{Ce}_{0.8}(\text{Y}_{1-x}\text{Ca}_x)_{0.2}\text{O}_2$  system decreases rapidly after CYC15. This could led to increasing activation energy of yttrium doped ceria and oxygen vacancy clustering.

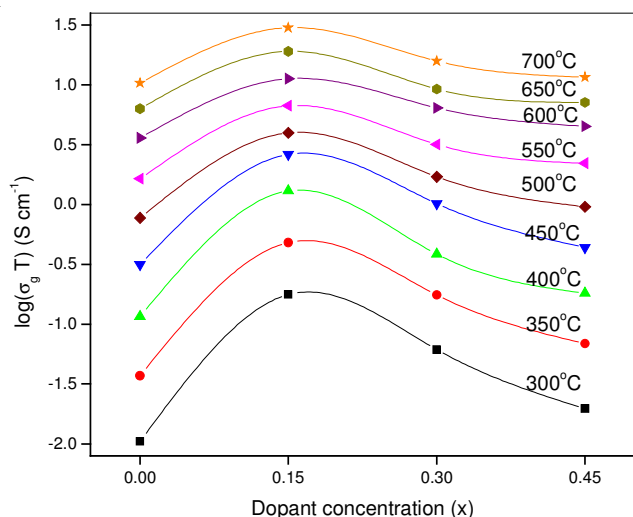


Fig. 8. Grain ionic conductivity isotherms as a function of calcium content (x) in  $\text{Ce}_{0.8}(\text{Y}_{1-x}\text{Ca}_x)_{0.2}\text{O}_2$  system

Fig. 9 shows the activation energy of  $\text{Ce}_{0.8}(\text{Y}_{1-x}\text{Ca}_x)_{0.2}\text{O}_2$  system for grain ionic conductivity as a function of dopant concentration (x). The activation energy values were calculated using least-squares method (Fig. 7). The correlation coefficients for linear fit lies over 0.9986, this indicates that the fit of the data is good. It is noticed that the activation energy is minimum for the CYC15 composition. This decrease in activation energy is due to the presence of attractive interactions between dopant cations and oxygen vacancies<sup>1</sup>. Stephens and Kilner<sup>19</sup> have observed similar results.

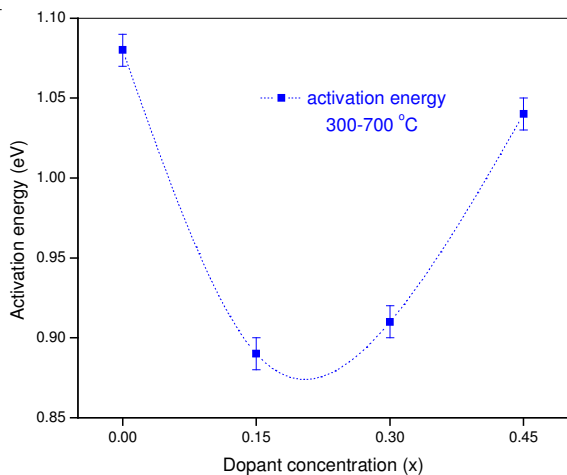


Fig. 9. Activation energy as a function of calcium content (x) in  $\text{Ce}_{0.8}(\text{Y}_{1-x}\text{Ca}_x)_{0.2}\text{O}_2$  system

Fig. 10 shows the thermal expansion of  $\text{Ce}_{0.8}(\text{Y}_{1-x}\text{Ca}_x)_{0.2}\text{O}_2$  in the temperature range 30–800 °C in air. From the Fig. 10, it is noticed that the thermal expansion curves are linear. The thermal expansion depends on the electrostatic forces within the lattice, which depend on the concentration of positive and negative charges and their distances within the lattice<sup>9</sup>. The thermal expansion coefficients (TEC) are calculated from the expansion curves using following expression:

$$\alpha_{\Delta T} = \frac{dL}{L \times \Delta T} \quad (6)$$

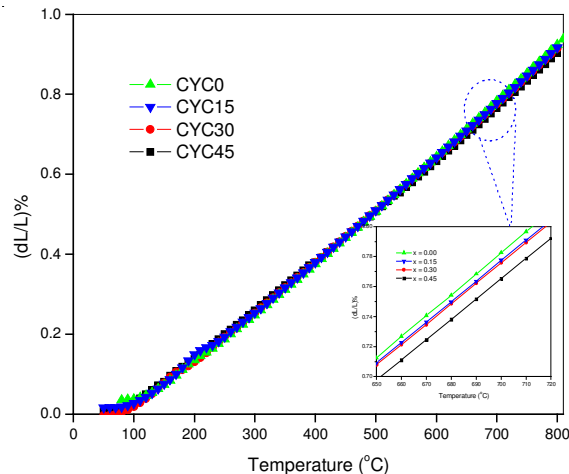


Fig. 10. Thermal expansion of  $\text{Ce}_{0.8}(\text{Y}_{1-x}\text{Ca}_x)_{0.2}\text{O}_2$  system

where  $\alpha_{\Delta T}$  is the average of thermal expansion coefficient in the temperature range of  $\Delta T$ ,  $dL$  is the change of sample's length in  $\Delta T$ ,  $L$  is the original length of sample.

The calculated thermal expansion coefficients are presented in Table-1. It is clear that thermal expansion coefficients are decreasing with the addition of Ca in  $\text{Ce}_{0.8}(\text{Y}_{1-x}\text{Ca}_x)_{0.2}\text{O}_2$ . It is noticed that  $T_{ec}$ 's change is very small. Results are in good agreement with the reported literature<sup>9</sup>. Further work is in progress to construct the solid oxide fuel cell and to study the application of this electrolyte.

TABLE-1  
THERMAL EXPANSION COEFFICIENTS  
(TEC) OF  $\text{Ce}_{0.8}(\text{Y}_{1-x}\text{Ca}_x)_{0.2}\text{O}_2$  SYSTEM

Composition	Nomenclature	TEC ( $10^{-6} \text{ } ^\circ\text{C}^{-1}$ )		
		600 °C	700 °C	800 °C
$\text{Ce}_{0.8}\text{Y}_{0.2}\text{O}_2$	YDC	11.54	12.01	12.23
$\text{Ce}_{0.8}(\text{Y}_{0.85}\text{Ca}_{0.15})_{0.2}\text{O}_2$	CYC15	11.31	11.81	12.02
$\text{Ce}_{0.8}(\text{Y}_{0.70}\text{Ca}_{0.30})_{0.2}\text{O}_2$	CYC30	11.24	11.63	11.91
$\text{Ce}_{0.8}(\text{Y}_{0.55}\text{Ca}_{0.45})_{0.2}\text{O}_2$	CYC45	11.03	11.32	11.70

## Conclusion

The co-doped ceria  $\text{Ce}_{0.8}(\text{Y}_{1-x}\text{Ca}_x)_{0.2}\text{O}_2$  samples were successfully prepared through the sol-gel process. Dense ceramics were obtained by sintering the pellets at 1300 °C and the results were consistent with the SEM analysis. The calculated relative densities were over 96 % of the theoretical densities. The lattice parameter varied linearly with an increase in Ca content. Thermal expansion coefficients of all the test samples are in the range  $(11.70\text{--}12.23) \times (10^{-6} \text{ } ^\circ\text{C}^{-1})$  at 800 °C. The grain ionic conductivity of  $\text{Ce}_{0.8}\text{Y}_{0.17}\text{Ca}_{0.03}\text{O}_2$  is 2.91 times higher than that of  $\text{Ce}_{0.8}\text{Y}_{0.2}\text{O}_2$  at 700 °C.

## ACKNOWLEDGEMENTS

One of the authors, Dr. S. Ramesh thanks the University Grants Commission (UGC), New Delhi, India for the financial assistance under DSKPDF scheme.

## REFERENCES

1. J.A. Kilner, *Solid State Ionics*, **129**, 13 (2000).
2. H. Inaba and H. Tagawa, *Solid State Ionics*, **83**, 1 (1996).
3. J. Neilsen, A. Hagen and Y.L. Liu, *Solid State Ionics*, **181**, 517 (2010).

4. C.S. Cheng, L. Zhang and S.P. Jiang, *Solid State Ionics*, **7**, 168 (2008).
5. S. Lubke and H.D. Wiemhofer, *Solid State Ionics*, **117**, 229 (1999).
6. N. Kim, B.H. Kim and D. Lee, *J. Power Sources*, **90**, 139 (2000).
7. Y. Liu, B. Li, X. Wei and W. Pan, *J. Am. Ceram. Soc.*, **91**, 3926 (2008).
8. S. Ramesh, C.V. Reddy, *Acta Phys. Polonica A*, **115**, 909 (2009).
9. S. Ramesh, V.P. Kumar, P. Kistaiah and C.V. Reddy, *Solid State Ionics*, **181**, 86 (2010).
10. F.Y. Wang, B.Z. Wan and S. Cheng, *J. Solid State Electrochem.*, **9**, 168 (2005).
11. S. Ramesh, K.C. James Raju and C.V. Reddy, *Trans. Indian Ceram. Soc.*, **70**, 143 (2011).
12. M. Dudek, A.A. Rapach-Kmita, M. Mroczkowska, M. Mosialek and G. Mordarsk, *Electrochim. Acta*, **55**, 4387 (2010).
13. T.S. Zhang, J. Ma, L.B. Kong, P. Hing, Y.J. Leng, S.H. Chan and J.A. Kilner, *J. Power Sources*, **124**, 39 (2003).
14. V. Epiosito, F.C. Fonseca, D.G. De Florio, M. Zunic, R. Miccillo and E. Traversa, *ECS Transactions*, **7**, 2093 (2007).
15. B.C.H. Steele, *Solid State Ionics*, **129**, 95 (2000).
16. R.D. Shannon, *Acta Cryst.*, **32A**, 751 (1976).
17. S. Omar, E.D. Wachsman and J.C. Nino, *Solid State Ionics*, **177**, 3199 (2006).
18. W. Lai and S.M. Haile, *J. Am. Ceram. Soc.*, **89**, 2979 (2005).
19. I.E.L. Stephens and J.A. Kilner, *Solid State Ionics*, **177**, 669 (2006).